Journal of Magnetic Resonance **143,** 161–171 (2000)
doi:10.1006/jmre.1999.1978, available online at http://www.idealibrary.com on IDEAL®

Burst Imaging: Rotation Artifacts and How to Correct Them

Claudia A. Wheeler-Kingshott,*[,1] Yannick Crémillieux,† and Simon J. Doran*

**Department of Physics, University of Surrey, Guildford GU2 5XH, United Kingdom; and †Laboratoire de RMN, UPRESA 5012 CNRS, Université Claude Bernard Lyon I, 69622 Villeurbanne Cedex, France*

Received July 20, 1999; revised November 8, 1999

The effect of coherent rotational motion on images acquired with the ultrafast single-shot spin-echo Burst sequence has been analyzed. Previous experience has demonstrated that sample rotation during Burst experiments has the potential to cause severe image artifacts. In this paper we show that no distortions are visible when the readout gradient is parallel to the rotation axis, but that there is a very distinctive behavior for the case of the rotation axis orthogonal to the imaging plane. The mathematical expression that describes the resulting signal is presented and is used as a basis for a method of correcting the *k*-space data. The conditions under which undistorted images may be recovered are discussed. It is shown that there is an asymmetry, dependent on the rotation direction, in both the manifestation of the artifact and the range of angular velocities over which one can correct the images. Data from an agar gel phantom rotating at a known rate are used to show how the theory is successful at reconstructing images, with no free parameters. The range of angular velocities over which correction is possible depends on the timing parameters of the pulse sequence, but for these data was $-0.016 < \omega \lesssim 0.1$ revolutions/s. Volunteer experiments have confirmed that the theory is applicable to patient motion and can correct motional distortion even when the exact rate is not known *a priori.* By optimizing the reconstruction to restore a known sample geometry/aspect ratio, an estimate of the rotation angular frequency is obtained with a precision of ±10%.

1. INTRODUCTION

From the early days of NMR it has been clear that the NMR signal is sensitive to both random molecular motion of the nuclear spins and coherent macroscopic motion (*1*). In the context of MRI, coherent motion can lead to image artifacts that seriously impair the diagnostic utility or quantitative accuracy of the data obtained (*2*). *In vivo* applications of MRI are particularly susceptible to this kind of distortion because of the natural respiratory and cardiac rhythms, pulsatile flow of blood and cerebrospinal fluid, and involuntary motion of the subject. There is a large body of work that examines the effects of motion on the various different MRI sequences (e.g., (*3, 4*)).

The use of ultrafast techniques, such as EPI (*5*), HASTE (*6*), snapshot-FLASH (*7*), GRASE (*8*), and spiral scan (*9*), characterized by total acquisition times of less than a second, can be a satisfactory solution to the problem of motion artifacts.

Burst (*10–13*) is an alternative ultrafast single-shot technique that has a number of specific advantages over the other previously mentioned sequences. These include: (i) an inherent insensitivity to magnetic susceptibility differences across the sample; (ii) low RF power deposition; (iii) low acoustic noise; (iv) less stringent system requirements (e.g., gradient rise times); (v) in-built diffusion contrast. Although Burst has a number of disadvantages, too, such as a relatively poor resolution and signal-to-noise ratio (SNR), it has considerable potential in certain niche areas, such as single-shot multislice imaging in regions where EPI can prove problematic due to susceptibility artifacts (for example, in the abdomen).

The inherent sensitivity of Burst methods to molecular diffusion (*14, 15*) led us to investigate how robust Burst is in the presence of macroscopic motion of the sample. This paper introduces a general formalism to explain the image artifacts induced by the sample rotation during Burst experiments and their possible correction, while further work (in progress) is looking at coherent translational motion and flow. The following issues will be addressed here:

- derivation of the general expression for the phase acquired by the spins in a sample rotating in the presence of a magnetic field gradient;
- description of the spin echo Burst sequence with an explanation of why the distortions in Burst images are different from those in images obtained with other sequences;
- application of the general expression for the phase to the special cases of a Burst experiment with the rotation axis perpendicular and parallel to the readout direction in the plane of imaging;
- explanation of the method used to correct the data;
- demonstration of the results obtained from phantom and *in vivo* experiments;
- discussion of the significance of the results obtained.

[1] Current address: NMR Research Unit, University Dept. of Clinical Neurology, Institute of Neurology, University College London, Queen Square, London WC1N 3BG.

1090-7807/00 $35.00

2. THEORY

2.1. General Remarks

It is well known that spins precessing in the presence of a magnetic field gradient, $\mathbf{G}(t)$, accumulate a phase, $\phi(t)$, associated with their position in the laboratory frame of reference, $\mathbf{R}(t)$, according to the integral

$$\phi(t) = -\gamma \int_0^t \mathbf{G}(t') \cdot \mathbf{R}(t')\, dt'. \quad [1]$$

Suppose that the sample rotates as a rigid body with an angular velocity $\omega(t)$. The spin's position $\mathbf{R}(t)$ in the laboratory frame of reference can be written (to a good approximation for $\omega t \lesssim 0.5$ rad) in terms of its fixed position $\mathbf{r}$ in the body frame of reference that rotates with the sample:

$$\mathbf{R}(t) = \mathbf{r} + \int_0^t \boldsymbol{\omega}(t') \times \mathbf{r}\, dt'. \quad [2]$$

Substituting this expression into Eq. [1] yields

$$\phi(t) = -\gamma \int_0^t \mathbf{G}(t') \cdot \mathbf{r} dt' - \gamma \int_0^t \mathbf{G}(t') \cdot \int_0^{t'} [\boldsymbol{\omega}(t'') \times \mathbf{r}]\, dt'' dt', \quad [3]$$

i.e., the phase accumulated by the spin can be split into two components, one of which depends on the position of the spin in the sample, while the other is an extra term introduced by the rotation. We may then employ the standard k-space notation with a new term $\mathbf{k}_{\text{rot}}$,

$$\phi(t) = \phi_0(t) + \phi_{\text{rot}}(t) = -(\mathbf{k} + \mathbf{k}_{\text{rot}}) \cdot \mathbf{r}. \quad [4]$$

Here $\mathbf{k} = \gamma \int_0^t \mathbf{G}(t')dt'$, as expected, while $\mathbf{k}_{\text{rot}}$ is found as suggested by Anderson and Gore (*16*) and reported in the following part of this section.

For suitably short times and/or small rotation angular velocities, we can replace $\int_0^{t'} [\omega(t'') \times \mathbf{r}]dt''$ with $\boldsymbol{\theta}(t') \times \mathbf{r}$, where $\boldsymbol{\theta}(t') = \int_0^{t'} \boldsymbol{\omega}(t'')dt''$ behaves approximately like a vector. Thus, the second term of [2] contains the vector triple product $\mathbf{G}(t') \cdot [\boldsymbol{\theta}(t') \times \mathbf{r}]$, which can be rearranged as $[\mathbf{G}(t') \times \boldsymbol{\theta}(t')] \cdot \mathbf{r}$.

Hence, comparing with [2] and [4],

$$\mathbf{k}_{\text{rot}} = \gamma \int_0^t \mathbf{G}(t') \times \boldsymbol{\theta}(t')\, dt', \quad [5]$$

and we are led to an expression for the NMR signal in the presence of rotation, $S_{\text{rot}}(\mathbf{k})$,

$$S_{\text{rot}}(\mathbf{k}) = \int_{\mathbf{R}} \rho_R(\mathbf{R}) e^{-i(\mathbf{k}+\mathbf{k}_{\text{rot}})\cdot\mathbf{r}}\, d^3\mathbf{R}, \quad [6]$$

where $\rho_R(\mathbf{R})$ is the spin density function in the laboratory frame and the integral is performed over the whole sample.

In the hypothesis of small angular displacements, one can assume that the spin density function does not change much passing from the laboratory to the body frame, thus $\rho_R(\mathbf{R}) \approx \rho_r(\mathbf{r})$. Since the element volume is the same in the two frames of reference, i.e., $d^3\mathbf{R} = d^3\mathbf{r}$, Eq. [6] becomes

$$S_{\text{rot}}(\mathbf{k}) = \int_{\mathbf{r}} \rho_r(\mathbf{r}) e^{-i(\mathbf{k}_{\text{rot}}+\mathbf{k})\cdot\mathbf{r}} d^3\mathbf{r}. \quad [7]$$

If $S(\mathbf{k})$ is the signal in the absence of rotation, then

$$S_{\text{rot}}(\mathbf{k}) = S(\mathbf{k} + \mathbf{k}_{\text{rot}}). \quad [8]$$

Thus, the effect of a small sample rotation in the presence of a gradient, $\mathbf{G}(t)$, is to shift the k-space signal, $S(\mathbf{k})$, corresponding to the ideal situation of a static sample, by the amount $-\mathbf{k}_{\text{rot}}$ (*16*).

2.2. The Burst Sequence

Figure 1 shows the Burst sequence diagram, while Table 1 explains the meaning of the variables used. In the following development, we choose the spin-echo Burst sequence (also known as DUFIS (*12*)), but with straightforward modifications; other Burst sequences may be analyzed. (In practice, our images have been acquired with the OUFIS phase modulation scheme (*13*), which increases the signal-to-noise ratio of the images, but this has no implications for the analysis presented.)

The main characteristic of the Burst sequence is the particular type of excitation: a train of n very short RF pulses is applied during a continuous gradient, along the read direction, to frequency encode the magnetization. A 180° slice-selective pulse, followed by a readout gradient of the same amplitude

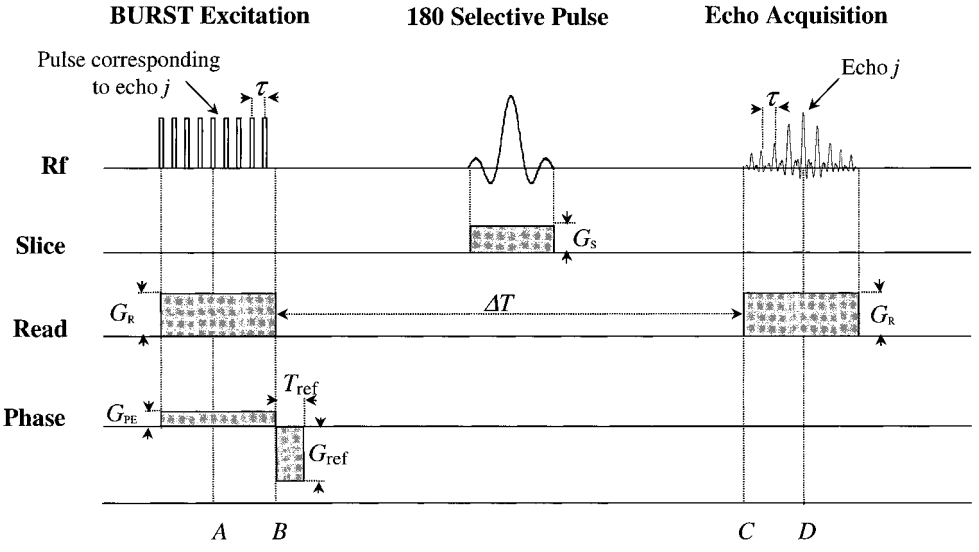

FIG. 1. Spin-echo Burst sequence. Each α-pulse of the Burst excitation pulse train creates a transverse magnetization that sees an excitation/readout gradient pair of a different length from the transverse magnetization created by the other pulses. The transverse magnetization created by the pulse that generates echo j experiences a read gradient from A to B and from C to D. The pulses can be considered independently one from the other if the linear approximation holds.

and duration as in the excitation period, refocuses a train of n spin echoes, one from each pulse. The phase encoding gradient is applied during the excitation too, and it is arranged to make each echo correspond to a different k-space line. A refocusing lobe determines the position of the central k-space line in the echo train.

In the hypothesis of independent pulses (linear approximation), it is possible to assume that the transverse magnetization created by each pulse experiences a read gradient of the same amplitude, but different length from that experienced by the transverse magnetization created by the other pulses. The same is true for the phase encode gradient. As is explained in the following sections, this difference in the gradient length is the source of a varying phase shift for the different lines of k-space data when sample motion occurs during data acquisition. Since only Burst-type sequences implement this gradient scheme, the motion artifacts that we analyze here are characteristic of these methods.

TABLE 1
Variables of SE Burst Used for Calculating the Position/Phase Shift of the k-Space Lines When in the Presence of Motion

Variable	Description
γ	Gyromagnetic ratio
n	No. of pulses (equal to the No. of echoes)
j	Echo No. ($j = 0, \ldots, n-1$)
n_R	No. of sampling points per echo (i.e., No. of pixels in the read direction)
t	Time variable
τ	Distance center-to-center between two successive α-pulses (echoes)
ΔT	Delay between the excitation and the readout gradients
T_{ref}	Length of the phase encode gradient lobe that determines the echo number for which $k_Y = 0$
A	Start of the excitation/PE gradient as seen by the pulse corresponding to echo j
B	End of the excitation/PE gradient
C	Start of the readout gradient
D	Center of echo j (i.e., spin rephasing $k_X = 0$)
G_R	Magnitude of the read gradient
G_S	Magnitude of the slice selective gradient
G_{PE}	Magnitude of the first lobe of the phase encode gradient
G_{ref}	Magnitude of the refocusing lobe of the phase encode gradient
ω	Rotation angular frequency

2.3. *Rotation Axis Perpendicular to the Readout Direction in the Plane of Imaging*

We shall consider first the case of a rotation whose axis is perpendicular to the imaging plane. As one might expect, this will entail considerable distortion since the object is moving along the large read gradient. Let us indicate with Z the axis of rotation, while X and Y are two orthogonal "in-plane" directions. θ_Z is, thus, the only component of the rotation angle which is different from zero. Let us assume also that the rotation has angular frequency, ω, constant over the time of the experiment and that the value $\theta_Z = \omega t$ satisfies the small angle condition described earlier. In this particular situation, the components $k_{rot,X}$, $k_{rot,Y}$, $k_{rot,Z}$ of $\mathbf{k}_{rot}$, deduced from Eq. [5], are reduced to

$$k_{\mathrm{rot},X} = +\gamma \int_0^t G_Y(t')\omega t' dt'$$

$$k_{\mathrm{rot},Y} = -\gamma \int_0^t G_X(t')\omega t' dt'.$$

$$k_{\mathrm{rot},Z} = 0 \qquad [9]$$

In order to apply Eq. [8], we write $G_X = G_{\mathrm{R}}$ (amplitude of the excitation and readout gradients) and $G_Y = G_{\mathrm{PE}}$ (amplitude of the phase encoding gradient).

In Fig. 1, the periods *AB* and *CD* represent, respectively, the dephasing and rephasing gradient lobes for echo *j*. *A* and *B* are also the starting and ending points of the first lobe of the PE gradient, as seen by the transverse magnetization that creates echo *j*. T_{ref} and G_{ref} are the length and amplitude of the phase encode lobe, applied immediately after excitation, that refocuses spins such that $k_Y = 0$ for the middle echo. The presence of the 180° refocusing pulse, midway between excitation and acquisition, inverts the phase of the spins and can be incorporated as a change in the sign of the initial gradients.

Under these assumptions, the formulae for the shifts can be written as

$$k_{\mathrm{rot},X} = -\gamma \int_A^B G_{\mathrm{PE}}(t)\omega t\ dt + \gamma \int_B^{B+T_{\mathrm{ref}}} G_{\mathrm{ref}}(t)\omega t\ dt$$

$$k_{\mathrm{rot},Y} = +\gamma \int_A^B G_{\mathrm{R}}(t)\omega t\ dt - \gamma \int_C^D G_{\mathrm{R}}(t)\omega t\ dt. \qquad [10]$$

If *n* is the total number of excitation pulses, τ is the separation center-to-center between two successive pulses and ΔT is the time between the end of the excitation and the beginning of the acquisition gradients, allowing slice selection to occur, then *A*, *B*, *C*, and *D* have the following expressions for the *j*th echo:

$$A = 0$$

$$B = \left(j + \frac{1}{2}\right)\tau$$

$$C = B + \Delta T = \left(j + \frac{1}{2}\right)\tau + \Delta T$$

$$D = C + B = 2\left(j + \frac{1}{2}\right)\tau + \Delta T. \qquad [11]$$

Note that the transverse magnetization contributing to echo *j* is created at point *A* and so $t = 0$ here by definition. The $\frac{1}{2}$ appears in the expression for *B*, *C*, and *D* because we consider times to the center of the *j*th echo.

TABLE 2
Parameters for SE-Burst Used to Perform the Rotation Experiments

Variable	Phantom	Volunteer
n	64	64
n_{R}	64	64
Field-of-view	120 mm	300 mm
Slice thickness	4 mm	10 mm
Bandwidth	100 kHz	100 kHz
τ	640 μs	640 μs
ΔT	17.36 ms	11.56 ms
Acquisition period	41 ms	41 ms
T_{ref}	2.5 ms	2 ms

Since *B*, *C*, and *D* depend on *j*, then $\mathbf{k}_{\mathrm{rot},X}$ and $\mathbf{k}_{\mathrm{rot},Y}$ are functions of the echo number, too. This means that the line of *k*-space corresponding to each acquired echo is shifted by a different amount, both along k_X and k_Y. We can calculate $k_{\mathrm{rot},X}$ and $k_{\mathrm{rot},Y}$ for the *j*th line in *k*-space by evaluating the formulae in [9] and [10] with the integration limits as defined in [11]. The shifts are both polynomial functions of the second order in the echo index *j*:

$$k_{\mathrm{rot},X} = a_X j^2 + b_X j + c_X$$

$$k_{\mathrm{rot},Y} = a_Y j^2 + b_Y j + c_Y, \qquad [12]$$

with the constants a_X, b_X, c_X and a_Y, b_Y, c_Y containing information about the gradient amplitudes and their duration (via the pulse separation τ). For detailed expressions see Appendix A. Evaluating the expressions for $k_{\mathrm{rot},X}$ and $k_{\mathrm{rot},Y}$, using parameters typical of Burst experiments (see Table 2) and the maximum rotation frequency in our phantom study (see Section 3), it turns out that $k_{\mathrm{rot},Y}$, which depends on G_{R}, is comparable to or even bigger than the separation Δk between *k*-space lines in absence of rotation, while $k_{\mathrm{rot},X}$ is negligible, being four orders of magnitude smaller than $k_{\mathrm{rot},Y}$. This underlines the predominant role of the excitation/readout gradient in determining the observed distortions.

2.4. Burst k-Space Data in the Presence of Rotation

From the previous sections, we have seen that the signal observed in a Burst experiment with a rotating sample is a shifted version of the correct signal, according to Eq. [8], and we have shown how to calculate what the *k*-space shift is. Figure 2 shows a representation of the shift along the phase encoding direction, k_Y, which is the more significant.

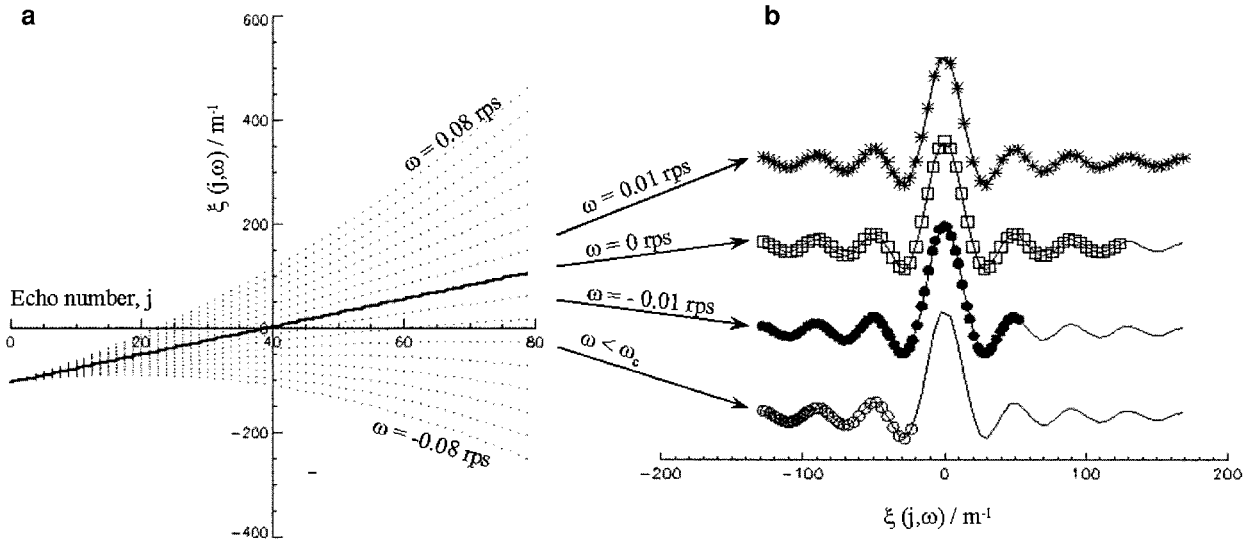

FIG. 2. (a) The function $\xi(j, \omega)$ vs the echo number j. The continuous line corresponds to the case of $\omega = 0$, while the dotted lines reflect what happens when $\omega = -0.08, -0.07, \ldots, 0.08$ rps. For large negative values of ω only the negative half of k-space is sampled, while for $\omega > 0$ the k-space lines are spread into the high positive frequencies. (b) The k-space profile along k_Y at $k_X = 0$ is plotted and compared for four different values of the rotation frequency: $\omega < \omega_c$, $\omega = -0.01$ rps ($\omega_c < \omega < 0$), $\omega = 0$, and $\omega = 0.01$ rps ($\omega > 0$). The k-space points are evenly and symmetrically sampled when $\omega = 0$. The presence of rotation with axis orthogonal to the readout direction of the image plane causes either oversampling of part of k-space ($\omega < 0$) or undersampling of the center of k-space with the data stretching further out, to cover higher positive frequencies ($\omega > 0$).

We define a function, $\xi(j, \omega)$,

$$\xi(j, \omega) = -[k_Y(j) + k_{\text{rot},Y}(j)], \qquad [13]$$

where $k_Y(j)$ is given by

$$k_Y(j) = -\gamma \int_0^B G_{\text{PE}}(t)\, dt + \gamma \int_B^{B+T_{\text{ref}}} G_{\text{ref}}(t)\, dt$$
$$= j\Delta k_Y + k_{Y_0}, \qquad [14]$$

and k_{Y_0} depends on the details of the phase encode blip, being used to position the central echo in k-space, while Δk_Y represents the step along k_Y in absence of rotation ($\omega = 0$). [The negative sign in Eq. [14] is purely for presentational purposes. Because of the effect of the 180° pulse, our k-space lines fill up from top to bottom (i.e., from positive k_Y to negative) with increasing echo number j. We feel that it is more intuitive, however, to visualize the experiment as running from negative to positive values, so that in Fig. 2 we can "read through" the experiment from left to right. We now refer to positive and negative halves of k-space according to this new convention.]

Using Eqs. [11] and [14] the function $\xi(j, \omega)$ can be written as

$$\xi(j, \omega) = -[a_Y j^2 + (b_Y + \Delta k_Y) j + (c_Y + k_{Y_0})] \qquad [15]$$

and thus depends on the echo number, j, and rotation frequency, ω, as shown in Fig. 2. The continuous thick line represents the case of $\omega = 0$, which means that the function $\xi(j, 0)$ coincides with $-k_Y(j)$. The dotted lines represent $\xi(j, \omega)$ for different rotation angular frequencies, from $\omega = -0.08$ revolutions per second (rps) to $\omega = 0.08$ rps. For $\omega > 0$, the faster the rotation is, the more $\xi(j, \omega)$ extends in the positive part of k-space, while for negative frequencies the coverage of the positive k-space is increasingly reduced until the signal is sampled only for negative values of k-space. We indicate with ω_c a critical negative frequency, corresponding to sampling one half of k-space plus at least $\frac{1}{8}$ of the lines of the other half, which is an oft-used minimum condition for "half-Fourier" image reconstruction (*17*). Appendix B derives an expression for ω_c and it is seen that this limiting value is dependent on the number of k-space lines acquired, n, and the sequence timing parameters, but not on the absolute value of the read gradient.

The effect of rotation is to cause the k-space lines to be either spread increasingly or compressed together. This is illustrated in Fig. 2b, where we have compared four different cases. The signal, obtained from simulated data, is plotted against $\xi(j, \omega)$, assuming the read gradient to be orthogonal to the rotation axis.

In each case, the continuous line shows the k-space data along k_Y at $k_X = 0$, for the ideal case of continuous symmetric sampling. The peak of the echo corresponds to the center of k-space. The discrete sampling points, represented by the function $\xi(j, \omega)$, have been overplotted and compared for $\omega = 0$ (the sampling points are uniformly distributed around the peak of the echo); $\omega > 0$ (the sampling points are increasingly

separated, resulting in an undersampling of the center of the echo and a coverage of k_Y, which extends to the high positive frequencies); $\omega_c < \omega < 0$ (there are only a few positive k_Y points because the data are sampled increasingly closer to each other, with more points than necessary at the center of the echo, but failing to sample some of the higher positive frequencies); $\omega < \omega_c < 0$ (the points are squashed together in the negative part of k_Y, missing completely the center and positive half of k-space).

2.5. Rotation Axis Parallel to the Readout Direction in the Plane of Imaging

When the readout gradient is parallel to the rotation axis, $G_X = G_s$ (slice-selection gradient) and $G_Y = G_{PE}$ or *vice versa.* By evaluating the expressions for $k_{rot,X}$ and $k_{rot,Y}$ in Eq. [8], we see that the effect of rotation is negligible in this case.

$k_{rot,X}$ is a polynomial function of the echo number j, as previously discussed, but for typical Burst parameters it is four orders of magnitude smaller than the regular k-space grid interval, Δk, that we would have in absence of rotation. $k_{rot,Y}$ is the result of the integral $\int_0^t G_s\ \omega\ t'\ dt'$ and so is a constant which does not depend on the echo number. The whole of k-space is shifted along k_Y by the same amount, which depends on the amplitude and length of the slice-selection gradient. For the minimum slice thickness we used and a typical gradient length, $k_{rot,Y}$ is three orders of magnitude smaller than Δk.

Other cases, in which the rotation axis is neither parallel nor perpendicular to the imaging plane, can be investigated using the same methodology. However, they will not be discussed further in this paper.

3. PHANTOM STUDY: METHOD AND RESULTS

The theory was tested by running the SE Burst sequence, optimized using Zha and Lowe's phase modulation scheme OUFIS (*13*), on a SMIS 2.0-T small bore scanner. SMIS (Guildford, England) provided a device to rotate a phantom along the axis of the magnet, indicated as Z, using a motor controlled by a frequency generator. A plastic cylinder of 5 cm diameter was filled with a gelatin type A, from porcine skin (approximately 300 bloom). A small plastic cylinder was inserted into the gel to create a pattern in the image. Two sets of experiments were carried out, with the parameters as in Table 2. The only difference was in the image orientation: in one case coronal slices were acquired, while in the other we sampled transverse slices.

Coronal orientation is obtained with the excitation/readout gradient along Z, therefore parallel to the rotation axis, while the phase encoding and slice-selection gradients are both orthogonal to the rotation axis. Transverse views are obtained with the excitation/readout gradient orthogonal to the rotation axis. In both cases, successive images were obtained at different values of ω, such that the small angle limit discussed earlier was adhered to (for a total imaging time of 100 ms, $0 \leq \theta_Z \leq 0.05$ rad).

Figure 3 shows the reference images ($\omega = 0$) and three other images acquired during the sample rotation ($\omega = 0.02$, 0.04, and 0.08 revolutions/s) for both orientations. As expected from the theory, no distortion is evident in the coronal images, confirming that, for small θ, the phase encoding and slice-selective gradients have negligible effects on the resulting rotation artifacts. The transverse images, however, do demonstrate rotation-induced artifacts, and these become increasingly evident as the rotation angular frequency increases.

The knowledge of the function $\xi(j, \omega)$ allows us to correct the artifacts in all of the cases studied here. Image analysis was carried out with IDL (Research Systems Inc., Boulder, CO). For each experimental case, the functions $\xi(j, \omega)$ and $k_Y(j)$ were evaluated using the appropriate values for the gradient amplitudes and duration, the number of Burst pulses implemented, and the image orientation. The angular frequency in $\xi(j, \omega)$ was passed by the user as a parameter either to be fixed to a known value or to be estimated (as in the volunteer study, discussed later).

The correction procedure was as follows:

- The input data were placed in a matrix S_{in}, such that $S_{in}(i, j)$ corresponded to the signal acquired at k-space point $(k_X(i), \xi(j, \omega))$.
- Data were taken from each column in turn and processed separately. Thus, we had a function s_i, sampled at the points $\xi(j, \omega)$. This function was interpolated to find its values at the points $k_Y(j)$. Note that, for $\omega > 0$, this involved "throwing away" the data for $\xi(j, \omega) > k_{Ymax}$. For $\omega < 0$, the high positive spatial frequencies were not acquired and it was necessary to zero-fill the output array.
- The interpolated data were then inserted into an output array $S_{out}(i, j)$, which was then Fourier transformed as normal to obtain the corrected image.

In the Discussion below, we comment in more detail on the performance of this method.

For the phantom study, the measured values of ω were used and so no free parameters were needed during the data processing. Figure 3 shows both the original and the processed images displayed one above the other. It can readily be seen that the gross geometric distortion of the images has been well corrected and that in the case of the $\omega = 0.08$ rps images there are other artifacts (particularly at the top and bottom rims) that have been successfully removed. Notice how the varying position of the circular black marker through the sequence of images shows that we are indeed seeing the sample at different points on the cycle as it moves around.

4. VOLUNTEER STUDY: METHOD AND RESULTS

In the previous section we have shown that knowing the function $\xi(j, \omega)$ allows the recovery of undistorted images

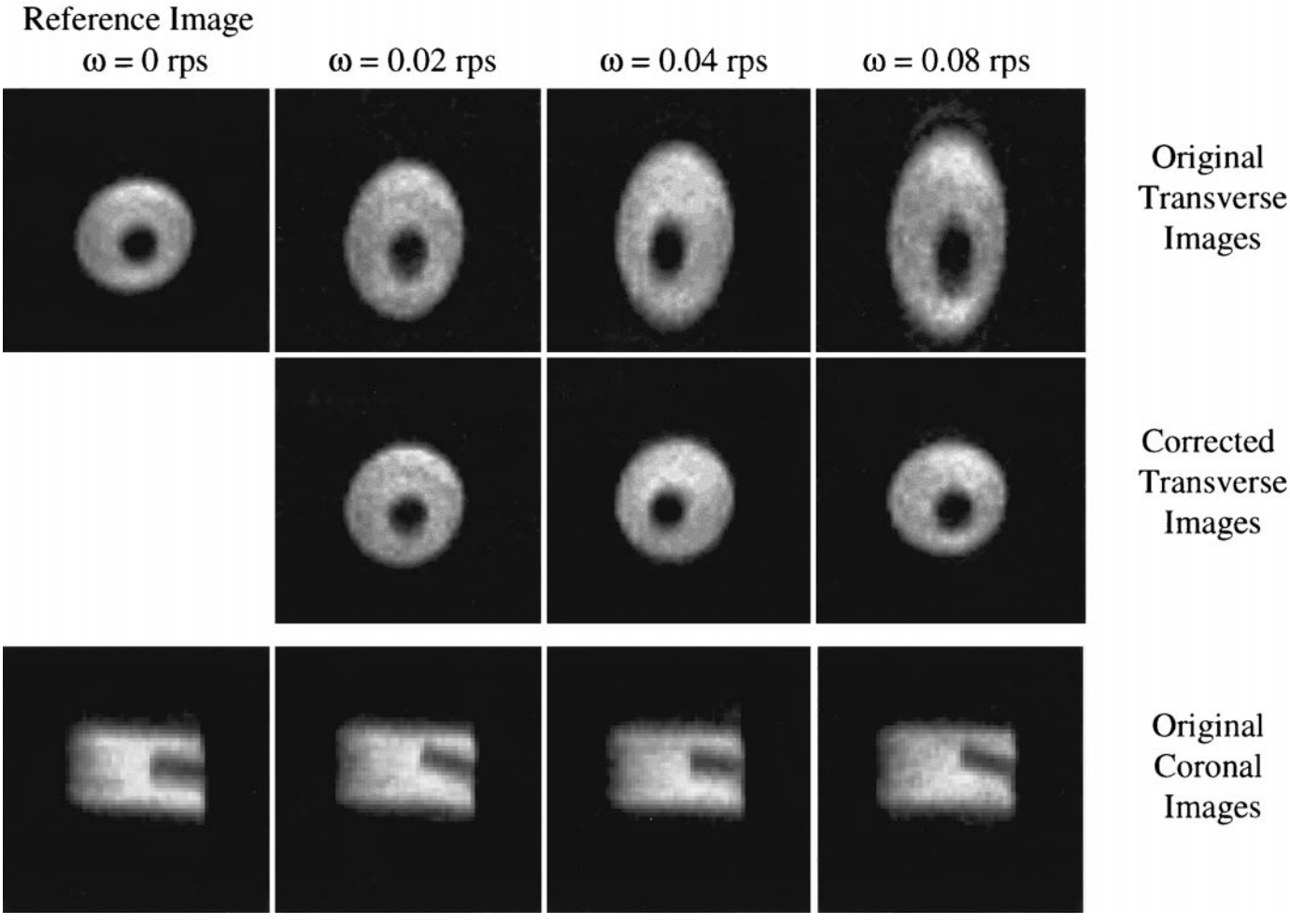

FIG. 3. SE Burst images of a gelatine phantom, acquired on a 2.0-T small-bore horizontal SMIS system. Transverse (top) and coronal (bottom) views are shown for different rotation frequencies: $\omega = 0, 0.02, 0.04, 0.08$ rps. For the coronal images the read gradient was parallel to the rotation axes and was not contributing to $k_{\mathrm{rot},x}$ and $k_{\mathrm{rot},y}$. Since the phase encoding has a small amplitude and the slice-select gradient is short, their contributions to the distortion are negligible. As expected, none of the images shows artifacts compared with the reference scan ($\omega = 0$). For the transverse slice, the read gradient was perpendicular to the rotation axis and the images show artifacts increasing with the rotation frequency. Below each transverse distorted image we have displayed the corresponding corrected one, obtained by Fourier transforming the data after reinterpolating it as described in the text. The only difference between scans is the position of the plastic tube in the gel which was inserted in the sample at an angle. Because the experiments were not triggered, the shots were acquired at different points of the rotation cycle.

when the rotation frequency is known. The question arises of how to correct the data when performing *in vivo* experiments where involuntary subject motion occurs. [In practice, such motions may not be the pure rotations to which we restrict ourselves in this section; we treat other cases in the Discussion below.]

A volunteer experiment was performed in which head images were acquired using a spin-echo Burst sequence on a 1.5-T Siemens Vision whole-body system. The volunteer controlled approximately the rotation speed and direction, being asked to turn his head either to the right or to the left and either slowly or rapidly. Both sagittal (rotation axis in the plane of the image) and transverse (rotation axis perpendicular to the imaging plane) images were acquired.

As expected the sagittal images (data not shown) demonstrated no distortion, but the rotation was evident from a changed position of the head in the images. Figure 4 shows the results from the transverse scans. Three images are displayed, corresponding to the three different k-space sampling situations of Fig. 2, together with a reference image ($\omega = 0$), in which the volunteer remained stationary in the scanner. As before, the images were corrected, but in this case, the true angular velocity of rotation was unknown and estimates were used. The function $\xi(j, \omega)$ was evaluated for a variety of values of ω and a trial reconstruction performed for each. We selected the rotation frequency that best reproduced the aspect ratio of the reference scan. The processed images are shown below the distorted images. It is evident that in two of the three

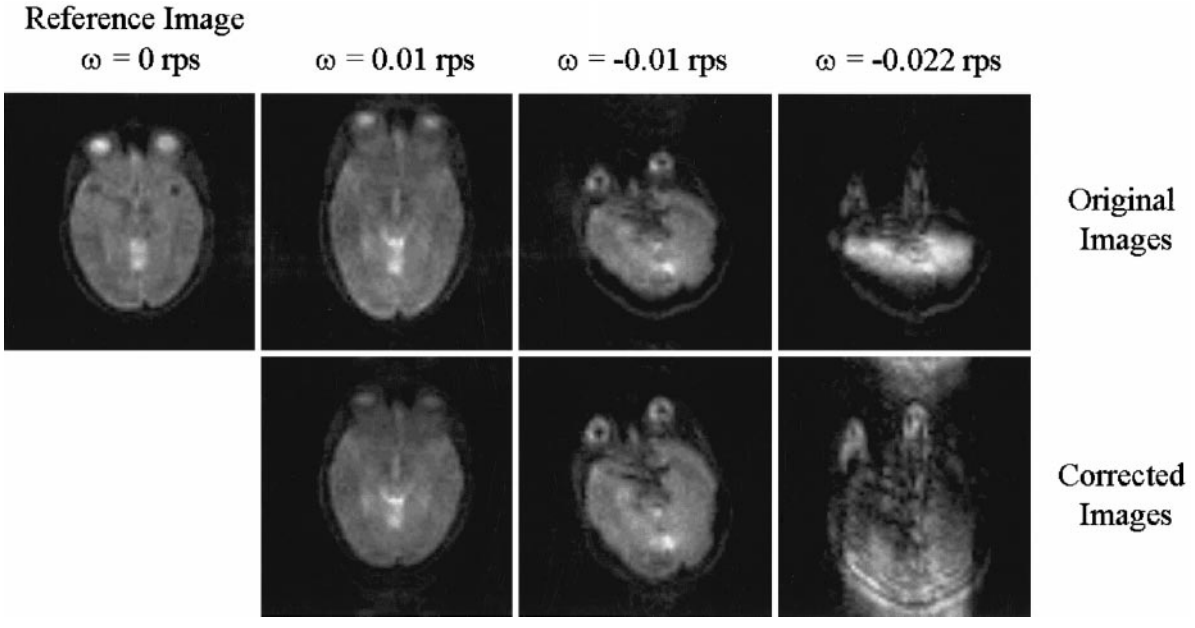

FIG. 4. Images of the human brain in the presence of rotation at 1.5 T. Original and corresponding corrected images are displayed one above the other. The reference scan corresponds to $\omega = 0$ rps. For $\omega > 0$, there is a complicated stretching artifact, but it is possible to recover the correct image. When $\omega_c \leq \omega \leq 0$ (see main text and Appendix B), there is a complicated compressional artifact, which is also correctable. When $\omega \leq \omega_c$, the low spatial frequencies are not acquired and the correction in this case is not possible.

cases, a successful correction is achieved, but in the case where $\omega < \omega_c$, it has not proved possible to correct the data. In the latter case, we see edge enhancements reminiscent of images that have been high-pass filtered and the origins of this effect are described further below.

5. DISCUSSION

During "conventional" experiments, such as spin echo and gradient echo, where the pulse sequence is repeated for each PE step, with the read and slice-selective gradients the same at each repetition, all lines of the *k*-space are affected in a similar way by a constant motion of the sample. By contrast, "fast" sequences that acquire all the lines in *k*-space in a single shot will suffer from a different phase shift for each *k*-space line. In the case of EPI, this phase shift is, in fact, relatively small, because the gradients oscillate rapidly and the phase accumulations tend to cancel out. This leads to a low sensitivity to motion. In the case of Burst, however, the excitation and read gradients have a constant sign, leading to rapidly increasing rotation-induced phase shifts. This is the origin of the characteristic distortion observed. Another low flip angle fast imaging technique, RUFIS (*18, 19*), overcomes this problem by sampling an FID immediately after each excitation, leaving little time for the phase accumulation, and thus exhibits much smaller rotation artifacts than Burst.

The phantom data confirm that it is possible to recover Burst images satisfactorily by employing the theory that we have developed. An *a priori* known rotation angular frequency was used to remap the nonuniformly spaced lines onto a *k*-space grid suitable for use with a fast Fourier transform. *In vivo* data, for which the rotation rate was unknown, were processed using a *guess* value for ω. The accurate knowledge of the anatomical details and dimensions was thus important for the outcome of the correction. The optimum rotation frequency was estimated to a precision of 10%, this figure being obtained by considering the rate of change in the corrected image dimensions as the trial value of ω was changed. However, with no independent means of measuring the angular velocity, we are unable to comment on the *accuracy* of the method. A modification of the Burst sequence to include a navigator echoes may be a feasible method of "building into" the sequence a way of deducing ω.

When the sample is rotating with a positive angular frequency, the data are acquired further into the positive half of *k*-space. The separation between adjacent *k*-space lines increases accordingly and this leads to the apparent decrease of the field-of-view (FOV) in the phase encoding direction, i.e., the vertical stretching in the uncorrected images of Figs. 3 and 4. This is not a simple stretching distortion, however, since the gap between adjacent k_Y lines is not constant.

The purpose of the current paper is to demonstrate and understand the distortion, rather than to develop an optimal correction method. Our current correction is rather crude and simply interpolates the data to the expected grid. There are two main consequences. For $\omega > 0$, the extra *k*-space lines are thrown away and the corrected image is undersampled. There is little that can be done for the loss of *k*-space sampling

resolution at the central spatial frequencies, but the additional positive *k*-space lines provide a potential means of increasing the image resolution by using an adaptive partial *k*-space technique.

In the case of negative angular frequency, the data are more clustered together, with the opposite effect of shrinking the image along the phase encoding direction. The distortion is as if a larger FOV, corresponding to a smaller *k*-space step, had been chosen. However, again, the asymmetry of the sampling in *k*-space means that we have more then a simple squashing of the image. The negative portion and the center of *k*-space are oversampled, but some of the positive higher spatial frequencies are missing altogether. Half-Fourier algorithms are strongly suggested to compensate for the asymmetric *k*-space sampling. The necessary data are lost completely if $\omega < \omega_c$, so that the image is high-pass filtered. Notice that, where less and less genuine *k*-space information is incorporated in the corrected image, there will be a decrease in SNR. This will be particularly dramatic when we no longer sample the center of *k*-space.

In this paper we have tackled the problem of rotation during Burst. Sample translation during acquisition will also affect the data and cause characteristic artifacts. The experimental verification of the effect of translation during Burst experiments is currently underway (*20*). Preliminary results are showing that, again, as expected, artifacts are significant only for the component of the translation along the read gradient. The data are modified by a nonuniform phase shift, related to the echo number, *j*, and the amplitude and duration of the read gradient. It is likely that correction using techniques like those above will be possible for a general rigid body motion composed of simultaneous translation and rotation. However, a limitation of the method may be our imperfect knowledge of the nature of the motion: without *a priori* information on the translational and angular velocities, corrections using the method above would become a matter of repeated trials, with results being evaluated on the basis of similarity to known/expected features of the image.

Two other situations are worthy of mention: nonrigid body motion and flow. The situation of nonrigid body motion is particularly complicated, with movement of the spins not describable by simple models. We suggest that image correction is likely to prove extremely difficult and probably not worth the effort. This would preclude the use of Burst in, for example, cine-cardiac imaging. (We have been able to obtain satisfactory single-shot Burst images within certain phases of the cardiac cycle, but at other points, the complexity and speed of the motion, of the order of 100-fold higher than the values studied here, make the data unrecoverable.) The case of flowing spins has also been investigated (*20*). Here, there is a distribution in velocities, rather than a simple bulk translation of the spins. In standard spin-echo, phase-contrast, velocity imaging, the velocity encoding period is short enough for these velocity differences to have minimal effects. However, in Burst experiments with a very long read gradient, an echo damping factor is introduced, which is related to the velocity dispersion.

6. CONCLUSION

Burst is an ultrafast single-shot imaging technique that can be seriously affected by motion artifacts, because of the large read gradients applied over a relatively long time. The transverse magnetization created by each pulse evolves under an excitation/read gradient pair of a different length. When the read gradient is orthogonal to the rotation axis, the resulting *k*-space is mapped to an irregular grid along k_Y. The artifacts are a result of naively Fourier transforming data as if it had been acquired correctly. As long as the acquired data cover a sufficient portion of *k*-space, the data can be corrected.

We have presented a simple model that allows images to be reconstructed even in the presence of moderate rotation. We have specified the limiting angular velocity beyond which data recovery becomes impossible. The method has been shown to work well when the rotation speed is a constant known *a priori,* and, as long as the sample aspect ratio is known, the correction succeeds even if ω is a parameter to be determined.

The rotation problem does not diminish the suitability of using Burst for fast effective scanning in the majority of cases. Burst retains all the advantages of a single-shot technique over conventional multishot experiments. An appropriate selection of the read gradient direction, coupled with suitable triggering, can reduce many of the effects of the motion, while processing using a scheme such as that described here can correct most residual motion.

APPENDIX A

Evaluation of $k_{\mathrm{rot},X}$ and $k_{\mathrm{rot},Y}$

In this Appendix we derive the formulae describing the effect of rotation during Burst experiments. For simplicity, the gradient ramps have been ignored for the calculations of the integrals, but it would be straightforward to include them.

We first recall some basic formulae relevant to Burst imaging. The read (and excitation) gradients are related to the image resolution ΔX by

$$G_{\mathrm{R}} = \frac{2\pi}{\gamma\, \Delta X\, \Delta t}, \qquad [A.1]$$

where Δt is the sampling interval. For isotropic image resolution from a Burst sequence with *n* echoes, each of which contains n_{R} points, and full *k*-space coverage (i.e., the same number of positive and negative lines), the following relations hold:

$$G_{PE} = \frac{G_R}{n_R} \qquad [A.2]$$

$$G_{ref} = \frac{1}{2} G_{PE}\left(n - \frac{1}{2}\right) \frac{\tau}{T_{ref}} = \frac{G_R\left(n - \frac{1}{2}\right)\tau}{2n_R T_{ref}}. \qquad [A.3]$$

Our starting expressions for calculating the motion terms are those for $\mathbf{k}_{rot}$ taken from Eq. [9] with values for A, B, C, and D substituted in from [11].

$$\begin{aligned} k_{rot,X} &= \gamma \int_0^{(j+1/2)\tau} G_{PE}(t)\ \omega\ t\ dt \\ &\quad - \gamma \int_{(j+1/2)\tau}^{(j+1/2)\tau+T_{ref}} G_{ref}(t)\ \omega\ t\ dt \\ k_{rot,Y} &= -\gamma \int_0^{(j+1/2)\tau} G_R(t)\ \omega\ t\ dt \\ &\quad + \gamma \int_{(j+1/2)\tau+\Delta t}^{2(j+1/2)\tau+\Delta t} G_R(t)\ \omega\ t\ dt. \end{aligned} \qquad [A.4]$$

After expanding the integrals, collecting together terms with different powers of j, and finally substituting for G_{PE} and G_{ref} in terms of G_R, we obtain the following expressions for the coefficients a_X, b_X, c_X, a_Y, b_Y, and c_Y of Eq. [11]:

$$a_X = -\frac{\gamma G_R \omega \tau^2}{2n_R} \qquad [A.5a]$$

$$b_X = \frac{\gamma G_R \omega \tau^2}{4n_R}(2n - 3) \qquad [A.5b]$$

$$c_X = \frac{\gamma G_R \omega \tau}{8n_R}[2(n-1)\tau + (2n-1)T_{ref}] \qquad [A.5c]$$

$$a_Y = -\gamma G_R \omega \tau^2 \qquad [A.5a']$$

$$b_Y = -\gamma G_R \omega \tau(\tau + \Delta T) \qquad [A.5b']$$

$$c_Y = -\frac{\gamma G_R \omega \tau}{4}(\tau + 2\Delta\tau). \qquad [A.5c']$$

Notice that all the Y coefficients are negative, but for presentation reasons we use $\xi = -(k_Y + k_{rot,Y})$ in the main text, hence the upwardly curving lines for positive ω in Fig. 2.

APPENDIX B

Evaluation of ω_c

The condition that at least $\frac{1}{8}$ of our lines are in the positive half of k-space, necessary if we are to reconstruct our data using partial Fourier techniques, translates into the expression

$$\xi(n, \omega) \geq \frac{n}{8} |\Delta k_Y|. \qquad [B.1]$$

The limiting negative value for which this is true is ω_c, where

$$\xi(n, \omega_c) = \frac{n}{8} \cdot \frac{\gamma G_R \tau}{n_R}, \qquad [B.2]$$

and we have substituted for $\Delta k_Y = \gamma G_{PE} \tau$ using [A.2]. Using Expressions [13], [14], and [A.2], we obtain

$$\gamma G_R \omega_c \tau \left[\tau n^2 + (\Delta T + \tau)n + \frac{1}{4}(\tau + 2\Delta T)\right] + \frac{n}{2}\frac{\gamma G_R \tau}{n_R} = \frac{n}{8}\frac{\gamma G_R \tau}{n_R}, \qquad [B.3]$$

where the last term on the LHS is $|n\Delta k_Y + k_{Y_0}|$ for an image with the phase-encode blip set to center the acquired data on $k_Y = 0$.

Rearranging leads to

$$\omega_c = \frac{-3n}{8n_R\left[\tau n^2 + (\Delta T + \tau)n + \frac{1}{4}(\tau + 2\Delta T)\right]}. \qquad [B.4]$$

For images with the parameters shown in Table 2, we obtain:

$$\omega_c(\text{phantom}) = -0.016 \text{ revolutions/s}^{-1}$$

$$\omega_c(\text{headscan}) = -0.018 \text{ revolutions/s}^{-1}$$

to 2 s.f. Notice that these values are dependent only on the sequence timings and, perhaps surprisingly, not on the image resolution via G_R. Notice also that, for $\omega > 0$, the locus of points obtained always passes through the central region of k-space (see Fig. 2). This means that it is possible to reconstruct images for much larger absolute values of angular velocity than $|\omega_c|$ when the rotation is in the positive sense. This is evidenced by the phantom results, where we can reconstruct images for $\omega = 0.08$ rps without significant loss of quality.

ACKNOWLEDGMENTS

The authors thank Prof. A. Briguet and Prof. M. Leach for the use of facilities at the University of Lyon and the Institute of Cancer Research,

respectively. SJD thanks Mr. J. Wolber for technical assistance and fruitful discussions. CWK thanks EPSRC for a studentship.

REFERENCES

1. E. L. Hahn, Spin echoes, *Phys. Rev.* **80,** 580–594 (1950).
2. R. M. Henkelman and M. J. Bronskill, Artifacts in magnetic resonance imaging, *Rev. Magn. Reson. Med.* **2**(1), 7–14 (1987).
3. R. J. Ordidge, P. Mansfield, and R. E. Coupland, Rapid biomedical imaging by NMR, *Br. J. Radiol.* **54,** 850–855 (1981).
4. E. M. Haake, Improving MR image quality in the presence of motion by using rephasing gradients, *Am. J. Roentgenol.* **148,** 1251–1258 (1987).
5. F. Schmitt, M. K. Stehling, and R. Turner, "Echo-Planar Imaging. Theory, Technique and Application." Springer-Verlag, Berlin (1998).
6. R. C. Semelka, N. L. Kelekis, D. Thomasson, M. A. Brown, and G. A. Laub, HASTE MR imaging: Description of technique and preliminary results in the abdomen, *J. Magn. Reson. Imaging* **6,** 698–699 (1996).
7. A. Haase, D. Matthaei, R. Bartkowski, E. Duhmke, and D. Leibfritz, Inversion recovery snapshot FLASH MR imaging, *J. Comput. Asst. Tomogr.* **13-6,** 1036–1040 (1989).
8. K. Oshio and D. A. Feinberg, GRASE (gradient-echo and spin-echo) imaging—A novel fast MRI technique, *Magn. Reson. Med.* **20**(2), 344–349 (1991).
9. A. N. Ahn, J. H. Kim, and Z. H. Cho, High speed spiral-scan echo planar NMR imaging, *IEEE Trans. Med. Imag.* **5-1,** 2–7 (1986).
10. J. Hennig and M. Mueri, Fast imaging using burst excitation pulses, *in* Abstracts of the Society of Magnetic Resonance in Medicine, 7th Annual Meeting, San Francisco, p. 238 (1988).
11. J. Hennig and M. Hodapp, Burst imaging, *Magma* **1,** 39–48 (1993).
12. I. J. Lowe and R. E. Wysong, DANTE ultrafast imaging sequence (DUFIS), *J. Magn. Reson. B* **101,** 106–109 (1993).
13. L. Zha and I. J. Lowe, Optimised ultra-fast imaging sequence (OUFIS), *Magn. Reson. Med.* **33,** 377–395 (1995).
14. S. J. Doran and M. Decorps, A robust, single-shot method for measuring diffusion coefficients using the burst sequence, *J. Magn. Reson. A* **117,** 311–316 (1995).
15. Y. Crémillieux, C. Wheeler-Kingshott, A. Briguet, and S. J. Doran, STEAM-burst: a single-shot, multi-slice imaging sequence without rapid gradient switching, *Magn. Reson. Med.* **38,** 645–652 (1997).
16. A. W. Anderson and J. C. Gore, Analysis and correction of motion artifacts in diffusion weighted imaging, *Magn. Reson. Med.* **32,** 379–387 (1994).
17. P. Margosian, F. Schmitt, and D. E. Purdy, Faster MR imaging: Imaging with half the data, *Health Care Instr.* **1,** 195–197 (1986).
18. D. P. Madio, H. M. Gach, and I. J. Lowe, Ultra-fast velocity imaging in stenotically produced turbulent jets using rufis, *Magn. Reson. Med.* **39,** 574–580 (1998).
19. H. M. Gach and I. J. Lowe, Observing curved flow using rufis, *Magn. Reson. Med.* **41,** 1258–1263 (1999).
20. C. A. Wheeler-Kingshott, "High Speed MRI: Analysis of new approaches to fast imaging using Burst-based sequences." Ph.D. thesis, University of Surrey (1998).